URSI AP-RASC, Sydney, Australia, 17 – 22 August 2025

First Commissioning Observation of LEKID camera at 100-GHz Band for Nobeyama 45-m Radio Telescope

H. Lee(1), S. Honda(2)(3), Y. Ishizaki(1), D. Cherouvrier(4), J. F. Macías-Pérez(4), A. Monfardini(5), N. Kuno(2)(3), A. Inoue(1), Y. Sato(1), R. Koriyama(1), Y. Murayama(6), M. Nagai(6), T. Nitta(2)(3), H. Matsuo(6), T. Oshima(6), Y. Sekimoto(7), N. Nakai(8)
(1) Degree Programs in Pure and Applied Sciences, Graduate School of Science and Technology, University of Tsukuba, e-mail: s2430053@u.tsukuba.ac.jp
(2) Division of Physics in Faculty of Pure and Applied Sciences, University of Tsukuba
(3) Tomonaga Center for the History of the Universe (TCHoU), University of Tsukuba
(4) Laboratoire de Physique Subatomique et de Cosmologie, Université Grenoble Alpes
(5) Institut Néel, CNRS and Université Grenoble Alpes
(6) Advanced Technology Center, National Astronomical Observatory of Japan
(7) Institute of Space and Astronautical Science, Japan Aerospace Exploration Agency
(8) School of Science and Technology, Kwansei Gakuin University

Abstract

We are developing a 100-GHz continuum camera with Microwave Kinetic Inductance Detectors (MKIDs) to be installed on the Nobeyama 45-m radio telescope in order to study star-forming regions and galaxies. In this study, a Lumped Element KID (LEKID) array was newly fabricated as the new focal plane detector. This LEKID array has 144 pixels with Hilbert meanders sensitive to the observation frequency of 100 GHz. After integration to the camera receiver was performed, the LEKID camera installed on the Nobeyama 45-m radio telescope in October 2024. This paper presents the results of laboratory performance evaluations and the first commissioning observations.

1. Introduction

Radio continuum observations in the millimeter-wave band play a crucial role in the study of galaxies and star-forming regions. For example, free-free emission from H_{II} regions, which are active star-forming regions, can be observed, allowing for the evaluation of star formation rates without being affected by dust absorption. Additionally, dust emission from distant galaxies can be detected, enabling the tracing of star formation activities that are difficult to observe in the optical and near-infrared bands. By combining observations at multiple wavelengths and determining the spectral energy distribution (SED), it is possible to estimate dust temperature and redshift, thereby investigating the process of star formation and galaxy evolution in the universe.

In recent years, the Microwave Kinetic Inductance Detector (MKID) [1], a superconducting resonator-based detector, has been increasingly used for wide-field and multipixel observations. We have developed the 100-GHz continuum camera and performed commissioning observations with the 109-pixel antenna-coupled MKID array [2,3]. The camera receiver has the vacuum window and large-aperture silicon lenses with anti-reflection (AR) sub-wavelength structures (SWS) to suppress surface reflection to below 1% in the 90-110 GHz frequency range [4] in order to pass the astronomical signals as much as possible. The dilution refrigerator (Taiyo Nippon Sanso Co.) with the Gifford-McMahon refrigerator (Sumitomo Heavy Industries, Ltd.) is used for cooling the MKID array below 200 mK.

In this study, the array of Lumped Element Kinetic Inductance Detectors (LEKIDs) [5] for this camera was newly developed. The LEKID employs a lumped-element circuit configuration using microstrip transmission lines and can be equivalently represented as LC resonant circuits, enabling the simultaneous readout of multiple pixels using a single readout line. Since the LEKID itself functions as an absorber, it does not require an antenna, making it more suitable for large-scale integration. The radiation absorbed in the LEKID generate quasiparticles by breaking Cooper pairs, which changes the resonance frequency. Therefore, the optical response of each pixel is measured by monitoring the shift of its resonance frequency. We integrated a 144-pix LEKID array into our camera receiver and conducted both laboratory performance evaluations and commissinoing observations using the Nobeyama 45-m radio telescope. The structure of this paper is as follows: Section 2 describes the fabricated LEKID array. Section 3 presents the beam size and noise performance as the laboratory evaluations. Section 4 shows the results of observations performed October 2024.

2. Detectors

The LEKID array was designed and fabricated in Université Grenoble-Alpes and the Néel Institute. Due to the advantage of large-scale integration, 144 pixels are packed into the array with a single readout line on the 3-inch silicon wafer, while the previous array has 109 pixels with planar antennas and silicon lenslets. LEKID pixel is designed with a microstrip line of an interdigitated capacitor shorted by a inductive line utilizing a Ti-Al bi-layer. The Hilbert meander is designed with inductive line as the absorption part sensitive to dual polarization similar to that used in the

NIKA camera [6]. The structure is optimized for the observation frequency of 100 GHz. The resonance frequencies of the LEKID array are tuned by adjusting the length of the interdigitated capacitor, resulting in readout frequencies ranging from approximately 650 to 900 MHz. Since the observation frequency of 100~GHz is the same as the antenna-coupled MKID array, LEKID array was installed at the optimized focus position confirmed by ZEMAX simulation and the same receiver optics is used for the observation. The designed LEKID array is summarized in Fig. 1. The readout system employs the 3-point modulation technique [9], developed at Université Grenoble-Alpes, for data acquisition. During the commissionning observations at the Nobeyama 45-m telescope, the receiver was successfully cooled to ∼150 mK.

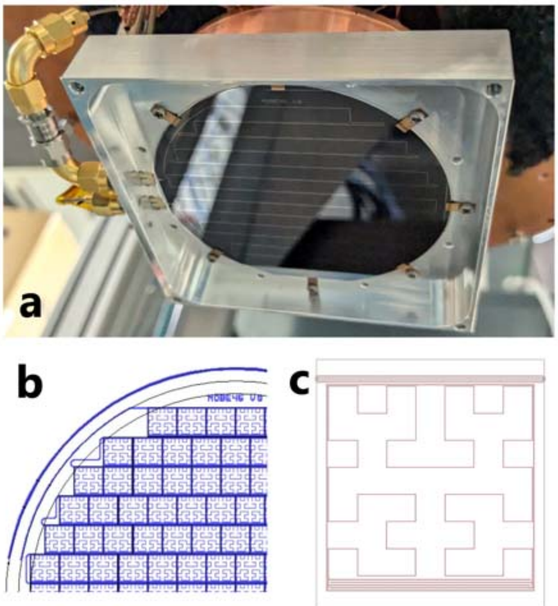

Figure 1. (a) 144-pix LEKID array mounted on the focal plane of the receiver. (b) A quarter section of the array, highlighting the structural layout. (c) A single LEKID pixel, showcasing the Hilbert meander structure. This design enables dual-polarization detection.

3. Lab measurement

The LEKID characteristics was evaluated in the laboratory at the Advanced Technology Center (ATC) of the NAOJ by using two radiation source in front of the receiver window, a room-temperature blackbody absorber (~300 K, hot load) and a blackbody cooled with liquid nitrogen (~77 K, cold load). Fig. 2 shows the feedline transmissions of LEKID resonators S_{21} with different optical sources, demonstrating the variation in the quasiparticle population. The 138/144 pixels are separated and show measurable responses, corresponding to a yield of approximately 95.8 %. The optical response was calculated with resonant frequencies of two optical sources.

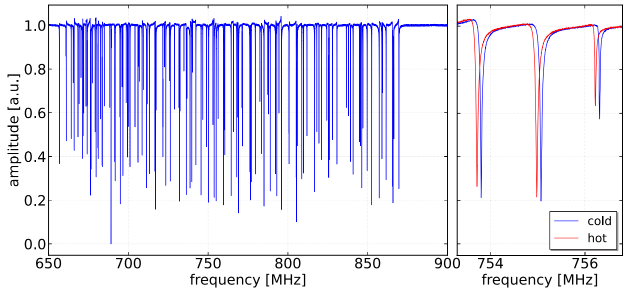

Figure 2. (a) Feedline transmission (S_{21}) of 138 out of 144 LEKID pixels with the cold (blue) and hot (red) loads. (b) Extracted view of three resonances with hot and cold loads, showing shifts of the resonant frequencies due to different radiation power.

3.1 Beam Pattern Measurement

The beam pattern was measured using the knife-edge method with a vector network analyzer (VNA) [7]. As illustrated in the left panel of Fig. 3, this method inserts hot-load plate between the receiver window and the cold load. The feedline transmissions of LEKID resonators were measured in 5 mm increments while recording the LEKID responses. The hot and cold loads were placed 2 cm and 10 cm below the receiver window, respectively. The actual measurement was performed by shifting the hot load in 5 mm increments while acquiring sweep data using the VNA. Measurements were taken along both the horizontal (x) and vertical (y) directions relative to the window. The obtained sweep data were used to derive the change in resonance frequency corresponding to the position of the hot load. Since the resonance shift follows the integral form of a Gaussian function, differentiation with respect to position yielded the beam profile (approximated as a Gaussian function) for each pixel. The distribution of the measured beam sizes is shown in the left panel of Fig. 4. The average beam sizes in the x and y directions were found to be 29.2±0.4 mm and 28.7±0.4 mm, respectively, which are in good agreement with the ZEMAX simulation prediction of approximately 30 mm. The right panel of Fig. 4 presents an array map correlating the beam positions with the corresponding LEKID pixels. The uniform distribution of beams indicates that the LEKIDs and the camera optics are functioning as expected.

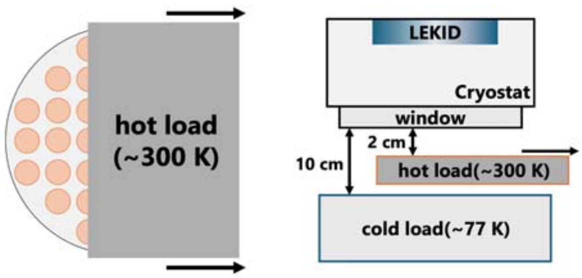

Figure 3. Schematic of the knife-edge method [7]. The obstruction slices through the beam pattern, and the optical response is measured. In this study, a hot load was used as the obstruction, and a cold load served as the radiation source.

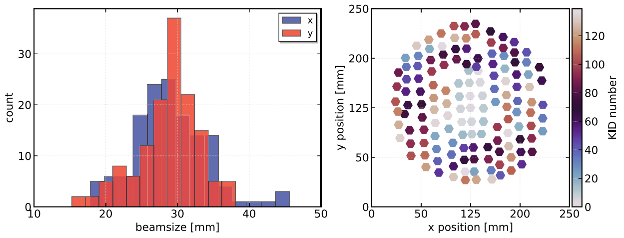

Figure 4. (Left) Distribution of measured beam sizes. Blue and red lines represent the x and y directions, respectively.Both directions yielded results consistent with the ZEMAX simulation prediction of 30 mm. (Right) Array map correlating the LEKID pixel numbers with their beam positions, showing a nearly uniform distribution as expected.

3.2 Noise Measurement

Noise measurements were conducted by acquiring time-ordered data (TOD) for individual pixels using a digitizer, from which the responsivity and noise characteristics were derived. The IQ mixer used in this study operates in the 2–8 GHz frequency range, whereas the LEKIDs resonate at 0.65–0.9 GHz. Therefore, a LO signal of 2.1 GHz was injected at the front and rear stages of the cryostat to perform frequency conversion. The radiation sources were identical to those used for the optical response measurements, utilizing both hot and cold loads. To separate system noise from LEKID noise, TOD measurements were taken at both on-resonance and off-resonance frequencies. Fig. 5 presents the measured noise PSD of the noise. The red and blue lines correspond to the hot and cold load measurements, respectively, while the gray line represents the off-resonance region. The on-resonance noise levels are higher than the off-resonance level, indicating the response of the LEKIDs.

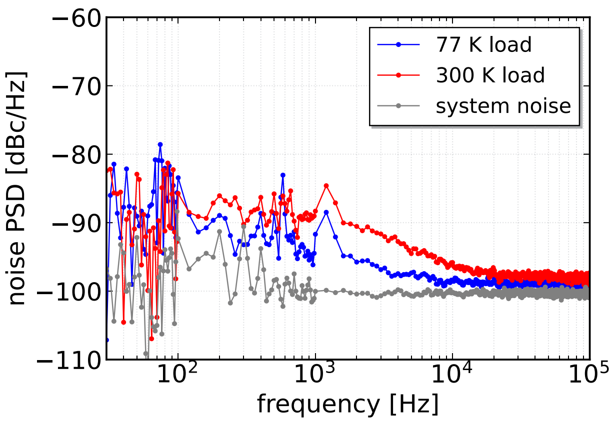

Figure 5. Noise PSD of a single LEKID pixel obtained in this measurement. The gray line represents the off-resonance noise, while the red and blue lines correspond to the hot and cold load measurements, respectively. The variation in white noise level due to radiation confirms the LEKID response. The roll-off observed around 10^3~Hz is attributed to the reduction in quasiparticle lifetime.

Comparing the hot and cold load results, the noise level difference corresponds to variations in radiation power, further confirming the LEKID response. Additionally, a roll-off in the white noise level was observed at frequencies $f \geq 10^3$ Hz, which is attributed to the reduced quasiparticle lifetime resulting from increased radiation power.

The PSD results shown in Fig. 5 were fitted for each pixel, and the white noise region around 100 Hz was used to calculate the noise equivalent power (NEP). The NEP values obtained from the hot and cold load measurements were $NEP_{\text{hot}} = 1.53 \times 10^{-15}\ \text{W}/\sqrt{\text{Hz}}$ and $NEP_{\text{cold}} = 7.54 \times 10^{-16}\ \text{W}/\sqrt{\text{Hz}}$, respectively. A comparison with the background-limited NEP (NEP_{BLIP}, BLIP: Background Limited Performance) is shown in Fig. 6. The NEP_{BLIP} is a calculated value derived from the incident power. Fig.6 indicates that the NEP obtained from the hot load measurement is close to the background-limited value. In contrast, for the cold load measurement, $NEP_{\text{BLIP}} < NEP_{\text{cold}}$, with a discrepancy of approximately 1.96 times. This saturation of noise could be attributed to stray light within the optical system. Additionally, as suggested by Fig. 5, the white noise level in the cold load measurement is slightly above the system noise, implying that system noise may be influencing the white noise level. Further investigation of stray light and system noise is required. However, considering the atmospheric temperature at the Nobeyama Observatory on clear days ~100 K, which is higher than the liquid nitrogen temperature of ~77 K, it is expected that observations approaching the background-limited level can be achieved.

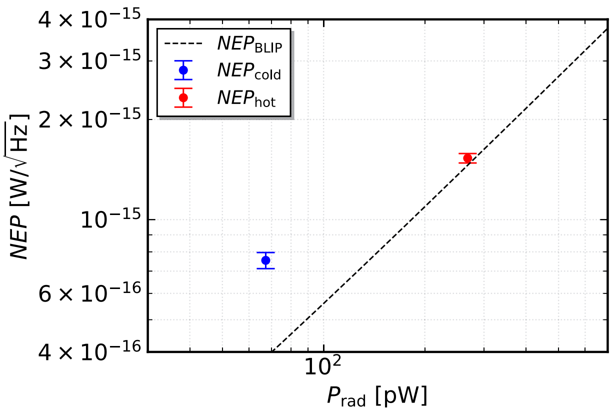

Figure 6. Comparison of NEP obtained in this measurement with NEP_{BLIP}. The red and blue points represent the NEP values for hot and cold load measurements, respectively. The dashed line indicates the NEP_{BLIP}. The hot load measurement shows NEP values close to the background-limited performance.

4. Commissioning

In October 2024, a commissioning observation was conducted using the 45-m radio telescope at the Nobeyama Radio Observatory of NAOJ. The observation campaign lasted for seven days, from October 17 to 24, accumulating a total of 50 hours of observation time. Raster scan observations were performed on planets (Mars, Jupiter, Saturn, Uranus), a radio source (3C 454.3), and galaxies (3C 84, M82, Cygnus A). In this study, the response of the KIDs was recorded as resonance circle data in the IQ plane. We used the NIKEL electronics derived from CONCERTO [8] for the readout system. The acquired data was converted into resonant frequency shift data through the 3-point modulation technique pipeline [9], which is also used in KISS [10]. Fig. 7 shows the beam maps for 3C 84, Saturn, Jupiter, and Mars obtained after this conversion for a single LEKID pixel. These beam maps represent different KID pixels, confirming that the beams appear at their corresponding positions within the array. Future work will include evaluating the beam pattern and sensitivity (NEFD) using planetary and 3C 84 data. Additionally, the observations of M82 and Cygnus A will be analyzed by stacking maps based on the beam pattern information obtained from this analysis.

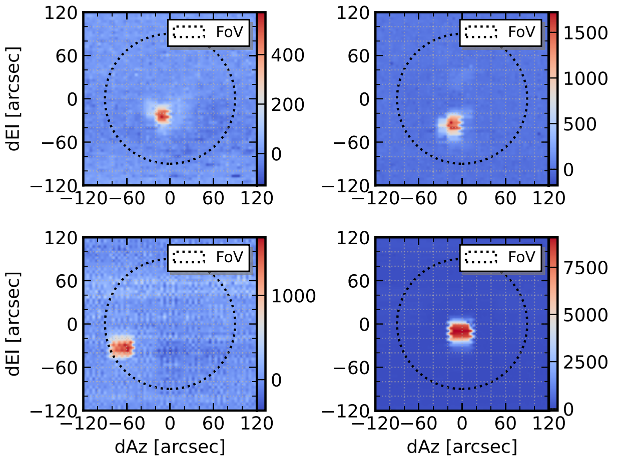

Figure 7. Beam maps drawn from converting raw observational data into frequency shift data. The results for 3C 84, Uranus, Mars, and Saturn are shown from the top left. Each map represents the on-source region ($4' \times 4'$) of the raster scan conducted during the observation. The color map indicates the magnitude of the frequency shift, while the circles within the maps represent the $3'$ field-of-view of the camera.

5. Conclusion

In this paper, we reported the results of laboratory evaluations and the commissioning observations of the 100-GHz LEKID camera installed on the Nobeyama 45-m radio telescope in 2024. In the laboratory measurements, the beam size obtained from the camera was found to be in good agreement with the values predicted by simulations. Additionally, the beam positions were distributed uniformly, consistent with the design expectations. The noise performance also showed that the hot load measurement reached values close to the background-limited level. During the commissioning observations, astronomical sources such as solar system planets and 3C 84 were successfully detected with a single pixel, and the beams were confirmed to appear at the corresponding positions within the array. Future work will involve analyzing the beam pattern and NEFD using the observational data and further examining the results of M82 and Cygnus A.
s

6. Acknowledgements

This study was conducted using the facilities of the ATC of NAOJ. We are deeply grateful to the staff of the Nobeyama Radio Observatory for their assistance in the installation and operation of the camera.

References

[1] P. Day, H. LeDuc, B. Mazin, A. Vayonakis, and J. Zmuidzinas, "A Broadband Superconducting Detector Suitable for Use in Large Arrays", *Nature,* **425**, October 2003, pp. 817-821.

[2] S. Honda, Y. Murayama, T. Nitta, M. Nagai, H. Miyazaw, et al., "Development and Commissioning of 100 GHz Microwave Kinetic Inductance Detector (MKID) Camera at the Nobeyama 45 m Telescope", URSI RADIO SCIENCE LETTERS, **4**, 2022.

[3] S. Honda, M. Nagai, Y. Murayama, H. Lee, Y. Ishizaki, et al., "Commissioning Observations in 2022 with 100-GHz MKID Camera at Nobeyama 45-m Telescope", 2023 XXXVth URSI GASS, August 2023, pp. 1-4.

[4] S. Doyle, J. Naylon, P. Mauskopf, A. Porch and C. Dunscombe, "Lumped Element Kinetic Inductance Detectors", *J. Low. Temp. Phys*., **151**, April 2008, pp. 530-536.

[5] T. Nitta, M. Nagai, Y. Murayama, R. Hikawa, R. Suzuki, et al., "Anti-Reflection Structures for Large-Aperture Cryogenic Lenses and Vacuum Window in 100-GHz Band", Millimeter, Submillimeter, and Far-Infrared Detectors and Instrumentation for Astronomy X, Online Only, December 14-18, 2020, p. 1145334C.

[6] M. Roesch, A. Benoit, A. Bideaud, N. Boudou, M. Calvo, et al., "Development of Lumped Element Kinetic Inductance Detectors for NIKA", ISSTT 2011 Workshop, December 2012, pp. 41-45.

[7] J. A. Arnaud, W. M. Hubbard, G. D. Mandeville, B. de la Clavière, E. A. Franke, and J. M. Franke, "Technique for Fast Measurement of Gaussian Laser Beam Parameters", *Applied Optics*, **10**, 12, December 1971, pp. 2775-2776.

[8] O. Bourrion, C. Hoarau, J. Bounmy, D. Tourres, C. Vescovi, et al., "CONCERTO: readout and control electronics", *Journal of Instrumentation*, **17**(10), October 2022, P10047.

[9] A. Fasano, J. F. Macías-Pérez, A. Benoit, M. Aguiar, A. Beelen, et al., "Accurate sky signal reconstruction for ground-based spectroscopy with kinetic inductance detectors", *A&A*, **656**, A116, December 2021.

[10] A. Fasano, M. Aguiar, A. Benoit, A. Bideaud, O. Bourrion, et al., "KISS: a spectrometric imager for millimetre cosmology", EPJ Web of Conference, **228**, January 2020.